Fluctuations in the excitation functions of dissipative collisions induced on the $^{27}Al+^{27}Al$ system in the laboratory energy range 114.2–123 MeV

M. Papa,[1,*] F. Amorini,[2] G. Cardella,[1] M. Cavallaro,[3] P. Figuera,[2] A. Musumarra,[3] G. Pappalardo,[2] F. Rizzo,[2] S. Romano,[2] S. Tudisco,[2] B. Heusch,[4] Wang Qi,[5] Si Songlin,[5] Lu Jun,[5] Tian Wendong,[5] and Hu Pengyu[5]

[1]*Istituto Nazionale Fisica Nucleare-Sezione di Catania, Corso Italia 57 95129, Italy*

[2]*Istituto Nazionale Fisica Nucleare-Laboratorio Nazionale del Sud, Via Santa Sofia 44, 95126 Catania, Italy*

[3]*Dipartimento di Fisica dell'Universita' di Catania, Corso Italia 57 95129, Italy*

[4]*Centre de Recherches Nucleares, F 67037 Strasbourg Cedex 2, France*

[5]*Institute of Modern Physics, Academia Sinica, Lanzhou, People's Republic of China*

(Received 10 March 1999; revised manuscript received 6 December 1999; published 22 March 2000)

The fluctuations in the excitation functions of the dissipative collision induced on the $^{27}Al+^{27}Al$ system have been studied in the laboratory energy range 114.2–123 MeV. The amplitude of the fluctuations, the average angular distributions, the energy autocorrelation functions, and the angular correlation functions have been studied in the framework of the partially overlapped molecular level model. The comparisons with the model allow us to estimate the characteristic times involved in the process, the degree of coherent rotations, and the density of molecular states through which the collision evolves. In particular the study of the angular correlations also reveals the coupling effects between rotational and intrinsic degree of freedom of the intermediate dinuclear system.

PACS number(s): 25.70.−z, 24.60.−k, 21.60.Ev

I. INTRODUCTION

The fluctuations of the excitation functions in dissipative binary heavy ion collisions (DBHIC) have been established since 1985 [1–4]. It is well known that an intermediate dinuclear system (IDS) is formed in DBHIC. The intermediate system does not attain complete statistical equilibrium within its lifetime; therefore, some obvious differences appear in this reaction mechanism in comparison to the process proceeding through a completely equilibrated compound nucleus (C.N.). The theoretical approaches developed for the phenomenon description of the phenomenon have tried to include modification with respect to the Ericson theory [5] to take into account some particular characteristics of the IDS like its deformation and the semiclassical rotation. These characteristics have been described by defining a space orientation for the system at the time of its formation and an average collective angular velocity.

In particular, the introduction of a correlation between different total angular momenta [6–11], which is necessary to produce the above mentioned effects, has shown that strong modifications appear in the *average angular distributions*, *energy autocorrelation functions* and *angular correlation function* with respect to the standard statistical theory describing the compound nucleus decay.

The effects of such a correlation are able to describe the behavior of many experimental data [12–15,20] characterized by (i) asymmetric average angular distribution with respect to 90° in the center-of-mass system (for nonsymmetric systems) showing in some cases a focusing effect; (ii) energy autocorrelation functions having in general a non-Lorentian shape with a strong angular dependence; or quasiperiodic structure connected with the rotation of the system.

Moreover, in all cases the mean level width of the IDS was found to be of the order of some hundreds of keV. This is a large value compared with the estimation performed according to the compound nucleus statistical theory, but on the other hand it is in agreement with the typical time of the deep inelastic process, $t \simeq 10^{-21}$s.

Until 1990 one problem remained unsolved: the fluctuations in the excitation functions are not washed out in spite of the high intrinsic excitation of IDS and of the enormous number of the final microstates contributing to the observable cross section in DBHIC.

Since 1991 the hypothesis that the fluctuating process evolves through a selective excitation of low density ''quasimolecular'' states embedded in a continuum of levels gave rise to the so-called partially overlapped molecular level model (POMLM) [16–19]. With this model we explained the visibility of the fluctuations and their main behavior. In Ref. [19] it has also been shown that the angular correlation function is able to give, together to the other quantities a stringent test for the model and for the relative approximations. In fact the angular correlation functions are closely connected with the square modulus of the Fourier transform (in the total angular momenta space) of the energy-averaged correlation amplitude and then it offers the possibility of investigating also the relative details.

Therefore, with the aim of testing the phenomenon and the POMLM more deeply, the DBHIC induced by the $^{27}Al+^{27}Al$ system have been investigated in the range 114.4–122.8 MeV in a wide angular range.

In Sec. II we describe the experimental apparatus and the data analysis. In Sec. III we present the results. Section IV is devoted to a review of POMLM, while in Sec. V we discuss the comparison between the experimental data and the model predictions. Section VI is devoted to the the comparison be-

*Electronic address: papa@lns.infn.it

tween the level density estimation performed according to the compound nucleus picture and the one obtained by the POMLM approach. Section VII contains the concluding remarks.

II. EXPERIMENTAL APPARATUS AND DATA ANALYSIS

A. Experimental setup

The experiment was performed at the SMP Tandem accelerator of the Laboratori Nazionali del Sud in Catania. An $^{27}Al^{8+}$ beam was used with a typical current of 40 nA and with energy from 114 MeV to 123 MeV in steps of 200 keV. A very thin target (around 40 $\mu g/cm^2$) was used in order to avoid a large energy spread of the beam in the target. The beam current was measured by an electron-suppressed Faraday cup, and the beam stability was checked on-line by using a monitor detector positioned at 5.8°. In particular the beam collimation system was made by two diaphragms which limited the beam disalignement to $\delta\theta_{lab}=\pm 0.15°$ and a third one was used as antiscattering ($\delta\theta_{lab}=\pm 2.5°$). The beam spot on the target was of the order of 2×2 mm^2. To cover a large angular range we used three telescopes consisting of a first stage transverse field ionization chamber, followed by a position sensitive silicon detector. The distances between the target and the detectors and the corresponding laboratory angular ranges covered were respectively $d_a=233$ mm: $10° \leqslant \theta_{al} \leqslant 22°$; $d_b=161$ mm: $22° \leqslant \theta_{bl} \leqslant 37°$; $d_c=160$ mm: $40° \leqslant \theta_{cl} \leqslant 58°$. In particular the telescopes a and c were placed at the right side with respect to the beam and telescope b was positioned on the left side.

The position information which had a resolution of ± 0.5 mm was used to determine the detection angle. Isobutane gas was used at a pressure of about 40 mbar. The calibration of the telescopes was performed by standard alpha sources and by various elastic peaks obtained by selecting different charge states from the Tandem beam. The gas detector was calibrated with the help of energy loss calculations and using calibration runs with and without gas in the detectors. The quality of the charge identification obtained can be evaluated from Fig. 1 where we show the ΔE-E scatter-plot for telescope b. Taking into account the beam spot and the position resolution, the geometrical angular resolution was about 1° in the laboratory.

B. Checks performed with the kinematical coincidences

The fundamental variable of the theoretical predictions on the phenomenon under study is the center-of-mass (c.m.) scattering angle θ of the primary fragments produced by the decay of the intermediate system. To estimate experimentally this variable, event by event, we have chosen the following criterion: when a projectlike fragment is detected, the measured laboratory angle, kinetic energy and the mass of the stable isotope having the atomic number of the identified fragment (our experimental setup does not allow the mass measurement) are used as input parameters to estimate the corresponding θ and Q value by use of the two body kinematical relations.

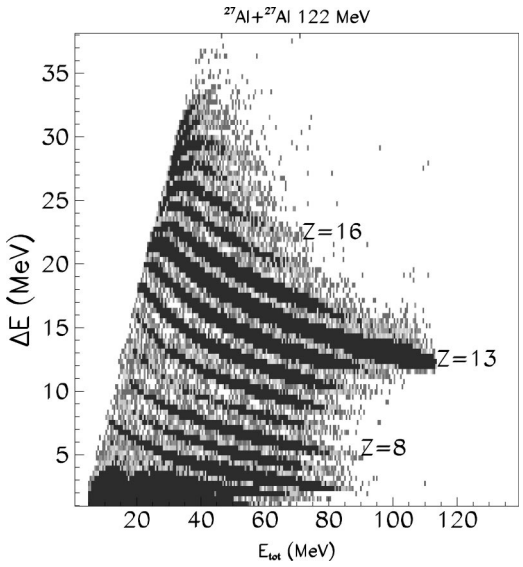

FIG. 1. ΔE-E_{tot} scatter-plot for telescope 2.

We observe, however, that this kind of estimation for the c.m. scattering angle can be affected by errors arising due both from the in-flight particle evaporation from the excited fragments and from the fluctuations of the total charge and mass partitions into the two primary fragments.

To evaluate the above mentioned errors we have analyzed the kinematical coincidences observed between projectilelike and targetlike fragments obtained from the detectors b and c placed on opposite sides with respect to the beam. In Fig. 2(a) we have plotted the center of mass angle $\theta_1-\theta_2$ scatter-plot relative to these coincidences for the total kinetic energy loss (TKEL) window 20–40 MeV. The c.m. scattering angles were determined by applying, in an independent way, the already quoted procedure to the two detected fragments.

From the figure it can be seen that the average of the two-dimensional distribution is centered around the line $\theta_1+\theta_2=180°$ as is expected for binary processes.

Moreover, from the projection—for example along θ_1 at fixed θ_2 of such a distribution [see Fig. 2(b)]—it is possible to evaluate the global average angular dispersion $\delta=\sqrt{\Delta\theta_1^2+\Delta\theta_2^2}$. In such a way, we can estimate for $\Delta\theta_1=\Delta\theta_2=\Delta\theta$ an effective angular resolution of about $\pm 4°$ in the center of mass system. We note that this value is larger than what may be estimated through the finite angular resolution in the laboratory system connected to the characteristic of the detection system.

The effects of the in-flight evaporation of the primary fragments has been investigated also by looking at the coincidence data.

In Fig. 3(a) we show the isotopic distribution measured for the binary coincidence events. If we add up the yields of all the isotopes with Z equal or lower than 13 and we moreover suppose the emission of a ^{27}Al primary source which decays by neutron, proton, and α particle emission, we obtain the following branching ratios: 48% of proton emission, 38% of neutron emission, and 14% of α emission. We note also the presence of Z larger than 13 indicating also a charge asymmetric breaking (44%) of the IDS due to the fluctua-

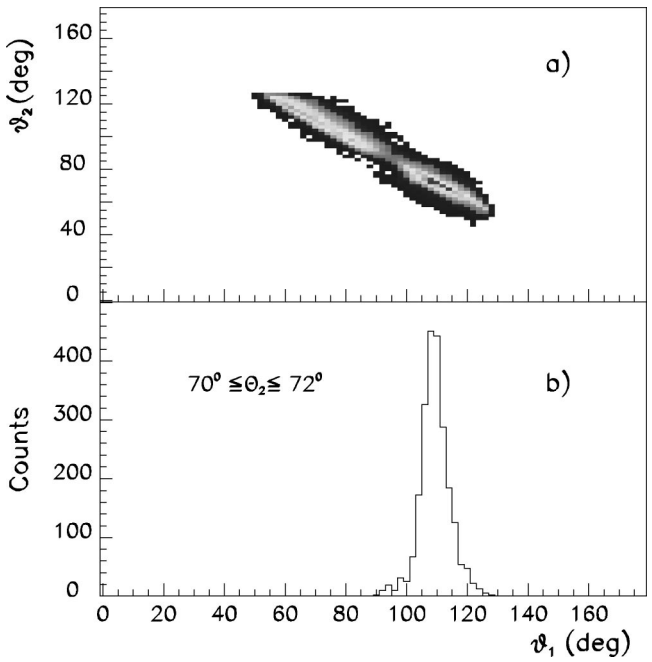

FIG. 2. (a) Scatter-plot of the c.m. angles for two coincident aluminium like fragments ($Z=11-14$) for the selected TKEL window (20–40 MeV). θ_1 is the c.m. angle of the heavier fragment (detected in the telescope b or c); θ_2 is the c.m. angle of the lighter (detected in the telescope b or c). (b) Projection of above scatter-plot along θ_1 coordinate for $70^\circ \leqslant \theta_2 \leqslant 72^\circ$. The FWHM of the spectrum can be connected with the effective experimental angular resolution (see the text).

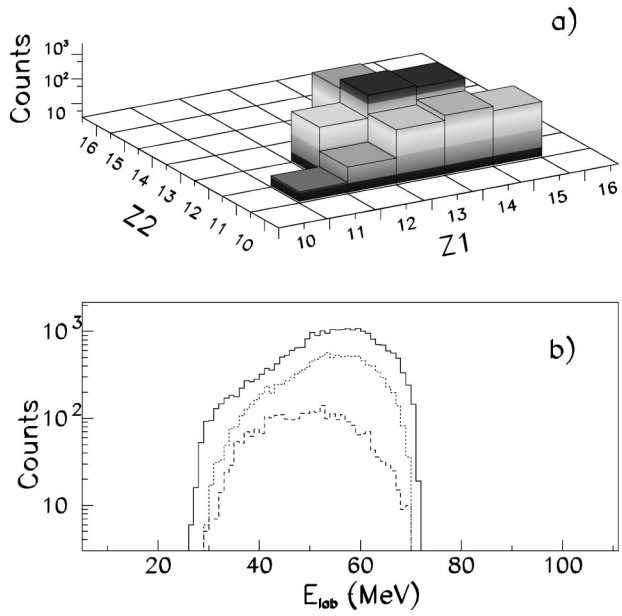

FIG. 3. (a) Two-dimensional distribution concerning the yield of binary coincidence as function of the atomic number of the fragments ($Z1$ for the heavier and $Z2$ for the lighter). (b) Laboratory energy spectra for $Z=13$ (continuous line) and $Z=12$ (dot line) fragments detected in the telescope b for single events. The dashed line represents the $Z=13$ spectrum collected for the binary coincidence events. The energy range corresponds to the TKEL window selected.

tions in the charge partition between the two primary fragments.

The previous estimated branching ratios roughly agree, with some minor difference of percentage, with CASCADE calculations [21] that we have performed on an ^{27}Al nucleus excited at an excitation energy of 15 MeV (we have considered an average TKEL of 30 MeV, the equal partition of the dissipated energy between the two partners and a maximum transferred spin of about 5 units of $\hbar$).

From these calculations, by taking into account the predicted particle energy spectra, we can evaluate an average recoil energy of about 0.2 MeV. This value is consistent with the above estimated angular dispersion. The indetermination on the estimated TKEL then is practically unaffected, on average, by the recoil energy but it is mostly determined by the propagation of the $\Delta\theta$ dispersion through the kinematical relations. This produces, for example, for $\theta=55^\circ$ and TKEL=15 MeV a dispersion of about ± 3 MeV.

Because we are analyzing inelastic process by single event data, the kinematical coincidence events have been used also to verify that spurious scattering from frames or slits does not affect the data collected with single quasialuminium events.

With this aim, we compare in Fig. 3(b) the $Z=13$ (continuous line) and $Z=12$ (dot line) laboratory energy spectra for single events detected in the telescope b. Their shape is practically identical. This evidence strongly supports the absence of scattering from frames. Moreover in the same figure we show, with a dashed line, the $Z=13$ spectrum collected for 2 quasi-aluminum coincidence events in the same telescope. The c.m. angular range is that covered by the kinematical coincidence for the TKEL window considered [see Fig. 2(a)]. The shape of the singles and coincidence aluminum spectra is similar; in particular the shape of the spectrum, related to single events, does not show the typical decreasing tail which is a characteristic of the energy degradation produced by the beam scattered from a frame. The difference in the yields comes both from the finite size of the detectors, for which binary events can be seen like a single one (because of the recoil effects due to the in-flight evaporation) and, more generally, from the fact that the binary coincidence events detected in a limited laboratory angle range ($\simeq 20^\circ - 58^\circ$ our experimental effective angular coverage for kinematical coincidence) are constrained by correlations in the θ-TKEL plane which are not valid in the single events as two body kinematical calculations show. These kind of checks have been performed for different runs at different incident energies.

C. Checks on carbon contamination

During the measurements, evidence of carbon contamination on the ^{27}Al target was observed. To evaluate the level of contamination we performed measurements at several incident energies also on a carbon target. To reduce the influence of the contamination in the data analysis, we have carefully studied the kinematics of the reaction for the binary dissipative reaction to eliminate all the events located in regions of

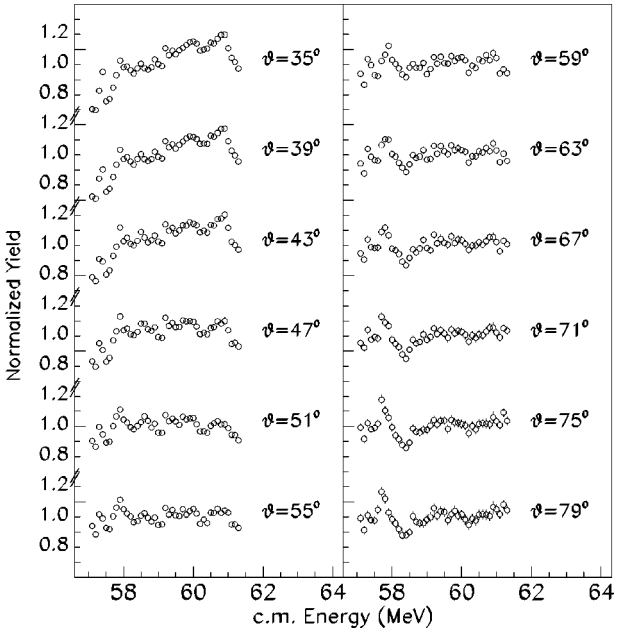

FIG. 4. Experimental excitation functions at different c.m. angles. To emphasize better the fluctuations the mean value of each excitation function has been normalized to unity.

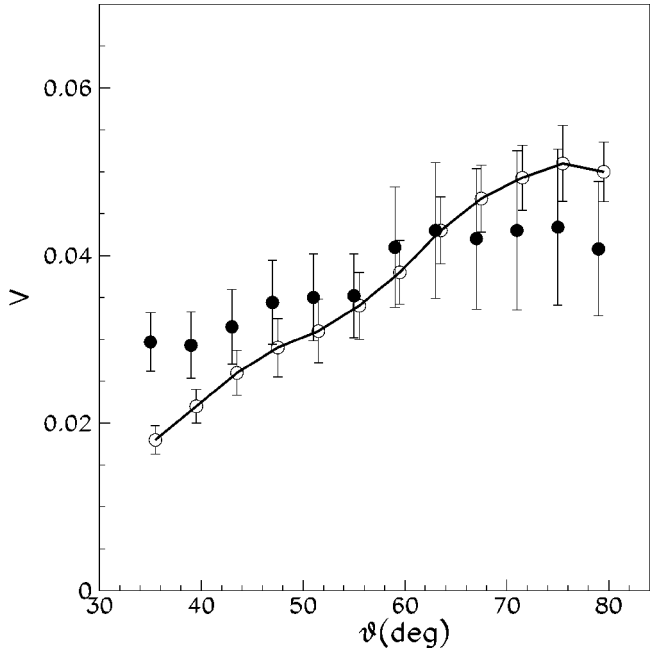

FIG. 5. Square root of the normalized variance V as function of the c.m. angles. The full dots represent the experimental values as deduced from the excitation functions shown in Fig. 4. The bars indicate the errors due to the counting statistics and to the FRD errors. The open dots joined with a continuous line (only to guide the eyes) represent the theoretical values as predicted by the POMLM (see text). The bars indicate the errors associated to the FRD effect.

the TKEL-$\theta_{\rm lab}$ plane where carbon contamination can be prominent (forward direction). Moreover this preliminary study is also important to determine a TKEL range for which the θ range accessible by our experimental setup is as wide as possible.

The result of such a study, with the above mentioned constraints, gives for the binary dissipative outgoing channels the following limitations: $\theta \geqslant 35°$, 20 MeV$\leqslant$TKEL $\leqslant$40 MeV and $Z=11-15$.

Inside this selected range and through the above mentioned measurements on the ^{12}C target, we have estimated an upper limit for the ^{12}C contamination level of about 20% at $\theta=35°$. This level rapidly and continuously decreases with angle and reaches a value lower than 8% for $\theta \geqslant 51°$.

D. Sum on different atomic numbers

In order to reduce the statistical error for the fluctuation analysis we have integrated all the charge yields from $Z=11$ to $Z=15$. This choice should not influence the description of our data for different reasons: (i) the study of the fluctuations in the excitation functions for the production of some particular isotope in the selected TKEL range, could be questionable because of the mixing of events generated by the in-flight evaporation of the excited particles; (ii) in previous works [1–4] it is shown that for nuclear charges near to the projectile ones, the difference in the extracted parameters is small; (iii) all the most recent theoretical approaches [16,17,19,22] which attempt to describe the phenomenon have not contained an explicit dependence on the particular class of outgoing channels selected. In other words the parameters governing these approaches depend only on the average time of the process and on the statistical properties of the intermediate system formed in the collision process (see Sec. IV).

Obviously changes of these properties can be expected if the selection criterion in data analysis are such that different reaction mechanisms are selected, but this is not the case in the present study because of the relatively narrow Q value and charge interval selected.

III. EXPERIMENTAL DATA

In Fig. 4 we show the c.m. excitation functions measured at different c.m. angles selected putting the appropriate conditions on the energy-position signals. They have been evaluated by a convolution procedure with a square window of half width equal to 4° on the excitation functions obtained by the primary analysis. The smoothing procedure has been applied on the basis of the measured effective experimental angular resolution (see Sec. II).

Quite large fluctuations are present well outside the error bars that are smaller or comparable to the point size. To emphasize the fluctuations better, we have normalized the mean value of each excitation function, to unity. The picture also shows an evolution of the cross section going from small to large angles. In particular the trend shows a marked dependence on the energy for $\theta \leqslant 51°$ which suggests the use of a recursive procedure to evaluate the average behavior [23]. This means, on the other hand, that the effective number of points of the excitation function available to characterize the fluctuations is reduced (several extrema points should be excluded from the analysis). In this case, in a practically equivalent way, we have chosen to analyze the

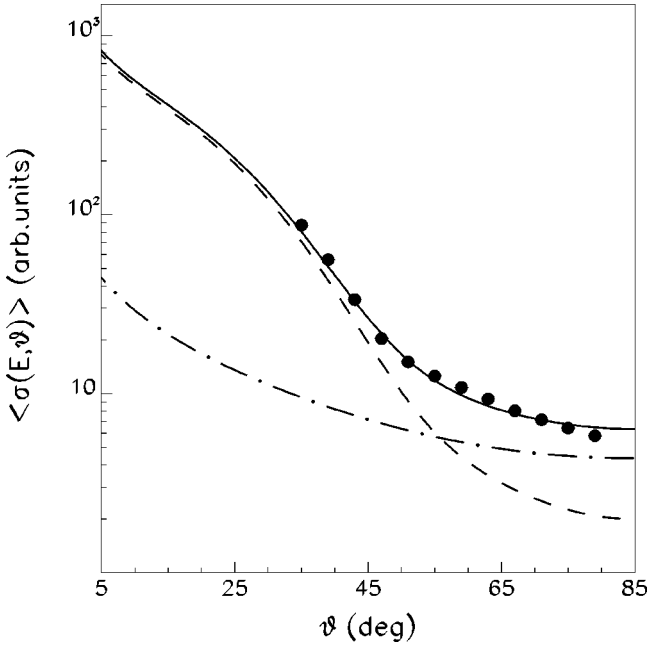

FIG. 6. Average angular distribution for the selected dissipative collisions. The full dots are the experimental data. The errors due to the statistics counting and those associated to the θ variable as due to characteristic of the detection system are comparable to the point size. The dot-dash and the dash lines represent the ''slow'' and ''fast'' contributions, respectively. The incoherent sum of these two components is drawn with a thick continuous line.

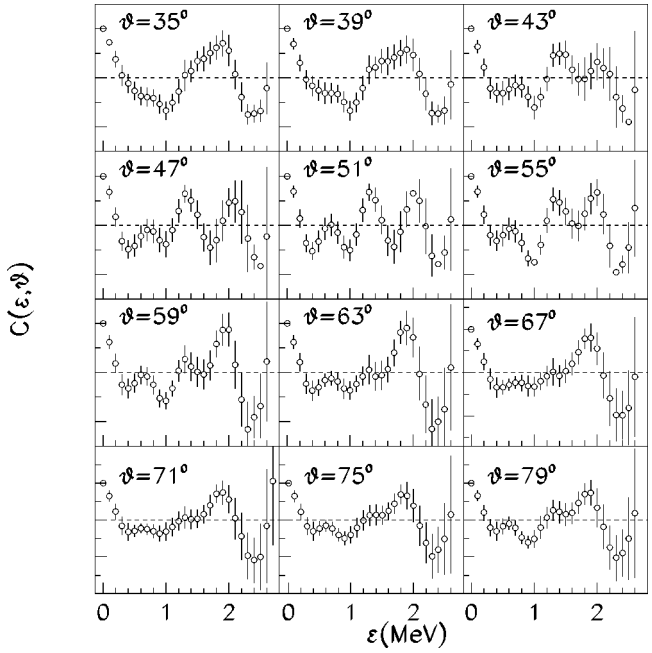

FIG. 7. Experimental normalized energy autocorrelation function at different c.m. angles.

fluctuations of the excitation function in the energy interval 58–60.9 MeV where the average yield is well represented by a linear, or at the most quadratic dependence, on the energy.

The square root of the normalized variance as function of θ is shown in Fig. 5 (full dots). The normalized variance has been evaluated according to the following expression:

$$V^2(\theta)=\frac{\langle(\sigma(E,\theta)-\langle\sigma(E,\theta)\rangle)^2\rangle}{\langle\sigma(E,\theta)\rangle^2}. \tag{1}$$

The brackets $\langle,\rangle$ indicate the average on the incident energy. The bars indicate the total error arising from the statistical uncertainty in the cross section and from the finite range of data (FRD). The FRD errors have been estimated in a model independent way by using the experimental quantities $\sigma(E_i,\theta)-\langle\sigma(E,\theta)\rangle$ (i is the running index on the energy step) and applying the error propagation procedure.

In Fig. 6 we report the experimental average angular distribution (full dots) [the lines represent theoretical calculations with the POMLM (see Sec. IV)]. The angular distributions show two different slopes at forward and backward angles in a similar manner to the $^{28}Si+^{28}Si$ system previously studied [19]. This behavior could be attributed to processes with different characteristic times as will be discussed in Sec. V. This evidence is also confirmed by the average trend of the excitation functions which, as already mentioned, at the forward angles display a visible energy variation.

In Fig. 7 we report the energy autocorrelation function $C(\varepsilon)$ at different c.m. angles:

$$C(\varepsilon,\theta)=\frac{\langle(\sigma(E+\varepsilon,\theta)-\langle\sigma(E,\theta)\rangle)(\sigma(E,\theta)-\langle\sigma(E,\theta)\rangle)\rangle}{\langle(\sigma(E,\theta)-\langle\sigma(E,\theta)\rangle)^2\rangle}. \tag{2}$$

The half-widths connected to the initial part of $C(\varepsilon)$ for the different angles are of the order of 150 keV$\pm$75 keV. Also in this case the bars indicate the error from the statistical counting and those connected to the FRD. In the whole angular range we note an increase of the correlation for ε around 2 MeV.

Finally in Figs. 8(a) and (b) we show the experimental angular correlation function (open dots) computed by taking as reference angles $\theta=67°$ and $\theta=55°$, respectively, according to the following expression:

$$C(\theta,\theta')=\frac{\langle(\sigma(E,\theta)-\langle\sigma(E,\theta)\rangle)(\sigma(E,\theta')-\langle\sigma(E,\theta')\rangle)\rangle}{\sqrt{\langle(\sigma(E,\theta)-\langle\sigma(E,\theta)\rangle)^2\rangle}\sqrt{\langle(\sigma(E,\theta')-\langle\sigma(E,\theta')\rangle)^2\rangle}}. \tag{3}$$

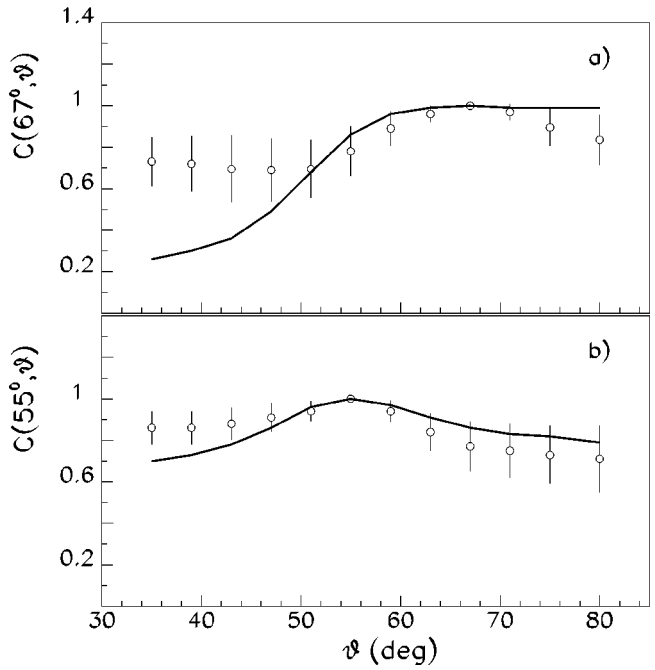

FIG. 8. (a) Experimental angular correlation function $C(67°,\theta)$ (points) compared with the POMLM prediction (continuous line). The bars indicate the errors due to the counting statistics and to the FRD. (b) Like (a) for $C(55°,\theta)$.

IV. REVIEW OF THE POMLM

As previously mentioned, the POMLM is a model that was developed to describe the fluctuations in the excitation function of dissipative heavy ion collisions [16,17]. We recall it briefly.

The starting point of the POMLM is a polar expansion of the S matrix connecting the initial channel α to each final channel β [6–11]. Through this expression the effect of the coherent rotation of the IDS has been taken into account in many previous works [7,10,12–14] to reproduce the experimental data. Accordingly the pole spectrum has the following structure:

$$E_\mu^{\rm pole}(J)=E_\mu^0+\frac{\hbar^2}{2I}J(J+1)-i\Gamma/2, \tag{4}$$

where I is the moment of inertia of the intermediate system and Γ is the mean value of the level width. E_μ^0 is the part of the resonant energy which is associated to other degrees of freedom than the rotational one. In this approach a sum over a very large number of final channels N is performed in an analytic way. The resulting total differential angular distribution has the following expression:

$$\sigma(E,\theta)=\frac{A}{\sin(\theta)}\sum_{J,J',\mu}(2J+1)(2J'+1)\times[W(J)W(J')]^{1/2}e^{i(\varphi(J)-\varphi(J'))}\times\frac{\overline{|b_{\alpha,\mu}|^2}P_J(\theta)P_{J'}(\theta)}{(E-E_\mu^{\rm pole}(J))(E-E_\mu^{\rm pole,*}(J'))}, \tag{5}$$

where

$$\overline{|b_{\alpha,\mu}|^2}=|\gamma_{\alpha,\mu}|^2\overline{|\gamma_{\mu,\beta}|^2}, \tag{6}$$

P_J indicates the Legendre polynomial of order J; $W(J)$ represents an effective transmission coefficient which is modelled with a Gaussian function centered around an average value $\bar{J}$ of the total angular momentum and a standard deviation $\Delta/\sqrt{2}$; $\varphi(J)=\Phi(\bar{J})(J-\bar{J})$ indicates the nonresonant phase shift associated with the scattering amplitude. As usual in this case the parameter Φ is connected, in the classical analogy, to the deflection angle corresponding to $\bar{J}$.

As can be observed the expression (5) is a coherent sum of different angular momenta. The degree of coherence is connected with the ratio $\gamma=\Gamma/\hbar\omega$ where ω is the average angular velocity of the IDS.

The expression (5) is derived in the Appendix through the following assumption on the amplitude $b_{\alpha,\mu}^\beta$: The numbers $b_{\alpha,\mu}^\beta$ are random variables characterized by the following properties: (i) $\langle b_{\alpha,\mu}^\beta\rangle=0;\overline{b_{\alpha,\mu}^\beta}=0$; (ii) $\overline{b_{\alpha,\mu}^\beta b_{\alpha,\mu'}^{\beta'}}=\delta_{\mu,\mu'}\delta_{\beta,\beta'}\overline{|b_{\alpha,\mu}^\beta|^2}i$. Here the brackets indicate, for each final channel, an average on the μ levels while the bar symbol indicates the average over the very large number of final channels N. The first condition reflects the statistical character of the process. The second assumption means that even if the correlation amplitude between two generic final channels β,β' can be different from zero, the average over all the very large number of distinct couples is zero. As shown in the Appendix this condition is equivalent to the resulting vanishing contribution (at the order $1/\sqrt{N}$) of the off-diagonal $\mu\ \mu'$ terms in the total cross section.

In Eq. (5) the ensemble average of the square modulus of the partial amplitude $b_{\alpha,\mu}$ is expressed through the random and uncorrelated reduced widths $\gamma_{\alpha,\mu}$, $\gamma_{\mu,\beta}$. In our calculations the average quantities $\overline{|\gamma_{\mu,\beta}|^2}$ are assumed to have a constant value which does not depend on the μ index. This property can be easily obtained if the fluctuation properties of each final microchannel β do not depend on the particular excited level μ of the intermediate system.

The analytical evaluation of the cross section correlation functions by means of the hypothesis which produce the expression (5) is a formidable task if the ratio between the mean level width Γ and the average spacing D of the levels has a value of the order of ten. In this case, in fact, the evaluation of the so-called ''four point functions'' [see the numerators of expressions (2) and (3)] of the S matrix would require a power expansion of S and the integration method based on the Grassman variables. Until now this method, resulting in very long calculations, has been applied only to the evaluation of the average correlation amplitudes and average cross section [24,25]. Therefore, in our approach, the expression (5) is evaluated by means of a Monte Carlo procedure from which the correlation functions can be easily computed. The numerical procedure has, on the other hand, two kinds of advantages:

(a) It allows us to overcome an approximation applied in the previous quoted approaches [$\bar{J}\simeq(J+J')/2$] which was done in order to obtain an analytic expression for the corre-

lation functions. This kind of approximation in fact hinders the spontaneous spread of the wave packet describing the coherent rotation of the intermediate system. Such a spontaneous spread becomes prominent in a time interval $\delta t(\mathrm{fm}) > (\hbar c/4\pi\hbar\omega\Delta^{2)}\bar{J}$ where $\bar{J},\omega,\ 1/2\Delta$ represent the average value of the total angular momentum, the average angular velocity, and the initial angular dispersion of the wave packet, respectively. This effect becomes relevant in the case of long-lived dinuclear systems.

(b) It is possible to properly compare the theoretical results with the experimental ones taking into account the distortions produced by the FRD errors.

In the Monte Carlo procedure the partial amplitudes $\gamma_{\alpha,\mu}$ of expression (5) are random number generated according to a Gaussian distribution with zero average. The level spectrum of the eigenvalue E_μ is obtained through a sequence of level spacings $D_{\mu,\mu+1}$ which are calculated under the assumption that the Hamiltonian random matrix elements are described by the Gaussian orthogonal ensemble statistics [26]. The resulting $D_{\mu,\mu+1}$ distribution is then the one parameter Wigner distribution characterized by the mean level spacing D.

An interesting result of this approach is that the cross section expressed through Eq. (5), in which the coherence between different total angular momenta is included, shows a fluctuating behavior comparable with the experimental one if the ratio Γ/D assumes a finite value [16,17], i.e., if the level density is low (some tens of MeV^{-1}). The hypothesis of a partial overlapping of the levels indicates that these states should be considered as special ones. In fact, as will be discussed in Sec. V A, the analysis of fluctuations for the system under study suggests that these states are located around 15 MeV above the ground state molecular band and that their estimated average density is much smaller than the value obtained through the well known level density formula obtained in the framework of a Fermi gas model.

Finally, we will briefly comment on the general behavior of the angular correlation functions and excitation functions and their connection with the structure of expression (5). This is the result of a study based on several calculations performed on the finite energy interval of measurement.

In the case of $\gamma \ll 1$, the off-diagonal elements $\sigma_{J,J'}$ in the J quantum number of expression (5) are overwhelmed by the corresponding diagonal one. This suppression is much higher than what can be expected from the low degree of angular momentum coherence, because these off-diagonal elements are, for $\Gamma \ll \hbar\omega$ and in the given molecular picture, out of the resonance for each level μ [see the denominators of expression (5)].

Therefore if interference between the near and far-side contributions is neglected, the model predicts in this case a high degree of angular correlation at all the angles $C(\theta,\theta') \simeq 1$, just because the changes of the excitation function with the angle arise only from the off-diagonal elements $\sigma_{J,J'}$.

If $\gamma > 1$, Monte Carlo simulations show that it is possible to select finite energy intervals of the order of 2–3 Γ in which the quasiperiodic structure of the excitation functions (the period is $2\hbar\omega$ for symmetric systems) becomes uncorrelated $[C(\theta,\theta') < 0.5]$ in angular ranges of the order of $1/\Delta$. These intervals must be located around the minimum of the wider disordered structures connected to mean lifetime of the intermediate system. In fact around these local minim the above mentioned off-diagonal terms become comparable to the diagonal ones and by involving different μ levels can be highly uncorrelated with the diagonal ones.

TABLE I. Values of the model parameters as obtained by means of the fit procedure for the ''slow'' and ''fast'' processes. They are the average deflection angle Φ (only fast process), the amplitude of the total spin windows Δ, the mean level width Γ_s, the angular momentum coherent length γ_f, the average rotational energy quanta $\hbar\omega$, and the average level spacing D (only slow process). The uncertainty intervals are also displayed.

Parameter	Best value	Uncertainty interval
γ_f	2.7	$\pm 10\%$
Δ_f	3.5	$\pm 10\%$
Φ_f	30°	$\pm 20\%$
$\hbar\omega$	1 MeV	$\pm 10\%$
Γ_s	0.5 MeV	0.3–0.6 MeV
Δ_s	2	1.5–4
Γ_s/D_s	13	10–40

V. COMPARISON WITH EXPERIMENTAL DATA

In this section we discuss the comparison between all the experimental quantities (already presented in Sec. III) which characterize the phenomenon and the POMLM predictions. The best fit procedure is rather complex because we have to describe, in a self-consistent way, all these experimental quantities.

Therefore we will describe in some detail the criterion used for the fit procedure, in this way we will also illustrate better both the physical meaning of the model parameters introduced in Sec. IV and the related dependence of the computed quantities. The parameters extracted from the fit procedure are displayed in Table I with the relative uncertainties.

A. Sum of the partial waves

As already mentioned, in all the calculations we have simulated the cross section given by expression (5). From the excitation functions we have computed the correlation functions and the normalized variance. For the average angular distributions we have analytically averaged the expression (5) on the incident energy E. Because of the symmetry of the system, the addition of the total angular momenta has been performed only for couple J,J' of quantum numbers having the same parity. Because of the relatively high TKEL considered in our process, quantal fluctuations of the reaction plane and the angular dispersion arising from the in-flight evaporation should destroy the effect of the near-far side interference [27]. This hypothesis is also confirmed by the absence of oscillations in the average angular distribution.

From these considerations, the following approximation has been performed in Eq. (5):

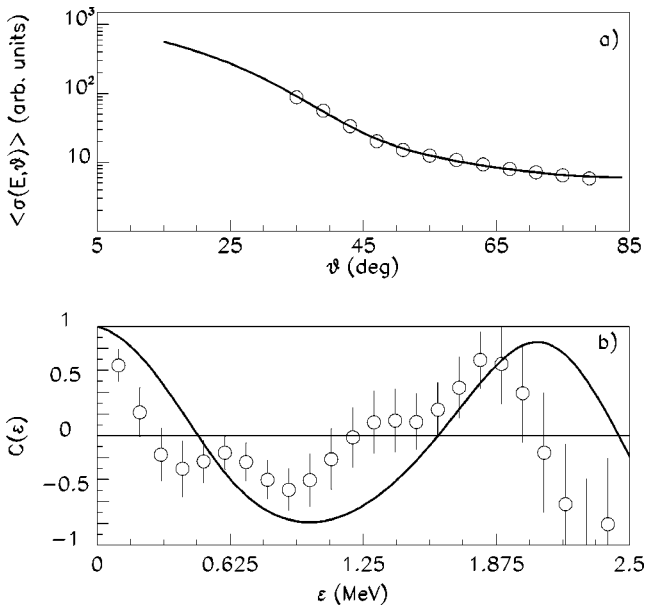

FIG. 9. (a) Average angular distribution fitted with the model predictions for one mechanism (continuous line). (b) The corresponding simulated energy autocorrelation function at $\theta = 75°$.

$$P_J(\theta)P_{J'}(\theta) \simeq \frac{1}{\sqrt{JJ'}}\cos(J-J')\theta. \tag{7}$$

B. Fast and slow components

The starting point of our analysis is the average angular distribution. In Fig. 9(a) we show the experimental quantities fitted with the model prediction in the case of one mechanism contributing to the process. The extracted γ parameter ($\gamma = \Gamma/\hbar\omega$) is about 1.2.

By taking 1 MeV as reference value of $\hbar\omega$ [19] (see also the following discussion on Sec. V D), the corresponding simulated energy autocorrelation computed at 75°, in the energy interval of analysis, is shown in Fig. 9(b) compared with the experimental one (points). The simulated autocorrelation looks different to the experimental one both with respect to a quantitative and a qualitative comparison. The apparent coherence length is about 0.3 MeV which is about two times greater than the experimental value. Moreover, in the relatively narrow interval of measurement (compared with the value of Γ) the simulated excitation functions of the single mechanism fit show a $2\hbar\omega$ quasiperiodic structure. This structure produces a smoothly oscillating energy autocorrelation function which is qualitatively different from the experimental one. The latter in fact displays narrow oscillations behind the bump centered at about 1.9 MeV. Apart from the smaller value of the coherence length, the presence of the narrow oscillation strongly suggests the presence of a statistical structure with a mean level width Γ smaller than 1 MeV (see Secs. V D and V F). It is possible to verify also that the behavior of the excitation function of the single mechanism process on a large energy interval $\Delta E \gg \Gamma$ is such that the quasiperiodic structures are overwhelmed by the statistical structure. This produces an energy autocorrelation that is characterized by a coherence length $\varepsilon_{1/2} \simeq \sqrt{2}\Delta\hbar\omega \simeq 3.4$ MeV, as the results of the space time localization of the IDS inside a width $d = 1/2\Delta$. These long-range energy structures produce, on the experimental energy interval, an average trend whose change with the energy is at least of the same order of magnitude as the amplitude of the quasiperiodic structure. This is not observed in our experimental data in the backward region, which shows a quite flat average trend compared with the amplitude of the fluctuations for angles greater than 51°. *A noticeable change of the average trend is instead observed at the smaller angles*.

All these considerations strongly suggest that two mechanisms are necessary to reproduce the data. Therefore in the following sections we will suppose that two incoherent processes, the so-called fast (f) and slow (s), act with different time scales

$$\sigma_T(E,\theta) = \sigma_f(E,\theta) + \sigma_s(E,\theta). \tag{8}$$

C. Average angular distribution and the fast process

The idea underlying the characterization of the whole phenomenon through two different times scales, as suggested from the experimental data, has the following consequences.

(i) The degree of angular momentum coherence of the two process must be very different, moreover, in our case, the γ's parameters must also be different from unity (see discussion in the previous section), that is $\gamma_f > 1$ and $\gamma_s < 1$. This means that the behavior of the angular distribution in the range $\theta = 35° - 53°$ will be mostly determined by the fast process while in the remaining explored angular range, in which a change of the slope is observed, the average angular distribution behavior will be determined by the gradual overwhelming of the slow process with respect to the fast one (see Fig. 6).

(ii) The amplitude and the behavior of the fluctuations for $\theta \geqslant 55°$ will be determined mostly by the slow process (see Sec. V).

In Fig. 6 we have already shown the results of the best fit on the average angular distribution (see also Table I). In Figs. 10(a)–10(c) we furthermore display the sensitivity of the theoretical total angular distribution to the parameters characterizing the fast process. The total average angular distribution weakly depends on the parameters describing the slow component. The procedure to determine them will be described in the following sections. In all the calculations shown in this section, the parameters of the slow process have been fixed to the values obtained from the global fit procedure and the continuous line represents the corresponding total contribution. The calculations corresponding to the changed parameters, whose values are shown in the figure, are represented by dashed lines.

In Fig. 10(a) we have changed the Δ_f parameter by $\pm 30\%$, around the value obtained from the fit ($\Delta = 3.5$). For the different curves the values of Δ_f are shown in the figure. The Δ parameter (see Sec. IV), being connected to the width $d = 1/2\Delta$ of the wave packet in the θ variable, determines the angular range in which a transition from a near-side scattering dominance (forward region) to a far-side scattering domi-

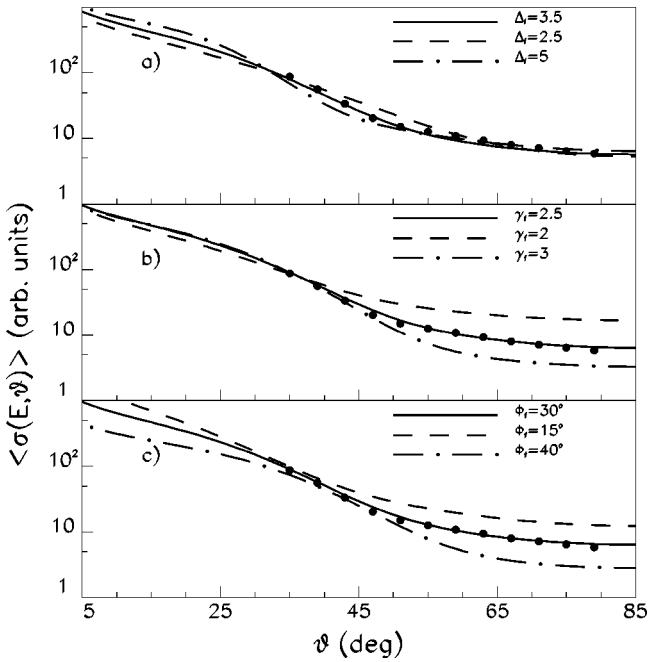

FIG. 10. (a) Total angular distribution computed for different values of the Δ_f parameter. The values of the parameter are reported in the figure. The continuous line represents the calculation obtained through the global fit procedure. (b) Like (a) but for different values of the γ_f parameter. (c) Like (a) but for different values of the Φ_f parameter.

nance is observed (backward region). The results shown by the curves plotted in the figure allow us to determine an uncertainty on this parameter of about $\pm 10\%$.

In Fig. 10(b) we display the results of the calculations in which the γ_f parameter has been changed by $\pm 10\%$ with respect to the value of 2.7 obtained from the fit procedure. This parameter determines the degree of coherent rotation and therefore also the ratio between the cross section around the angle Φ (near-side dominance) and the cross section at the backward angle (far-side dominance). The curves plotted in the figure allow us to determine an uncertainty on the γ_f parameter of about 10%.

In Fig. 10(c) we show the results of the same procedure for the Φ_f parameter which defines the orientation of the intermediate system at $t \simeq 0$ [14]. In this case we evaluate an uncertainty of about $\pm 20\%$.

We observe also that because of the relatively narrow interval of measurement compared with the energy coherence length of the fast process, we cannot determine both the $\hbar\omega_f$ value connected to this process neither the value of Γ_f. In any case, it is clear that, with the reasonable assumption of $\hbar\omega_f \geqslant \hbar\omega_s$, the following relation holds: $\Gamma_f \geqslant \gamma_f \hbar\omega_s$.

The parameters of the slow process will be determined instead by the description of the main behavior of the fluctuations. This makes it necessary to fix the energy scales and therefore the time scale of our process. To do this, in turn, we have to estimate the $\hbar\omega$ parameter (in the following $\hbar\omega$ will indicate $\hbar\omega_s$). Before discussing this subject, in the next section we illustrate the final results obtained on the energy autocorrelation function in the backward angular region as obtained through the fit procedure.

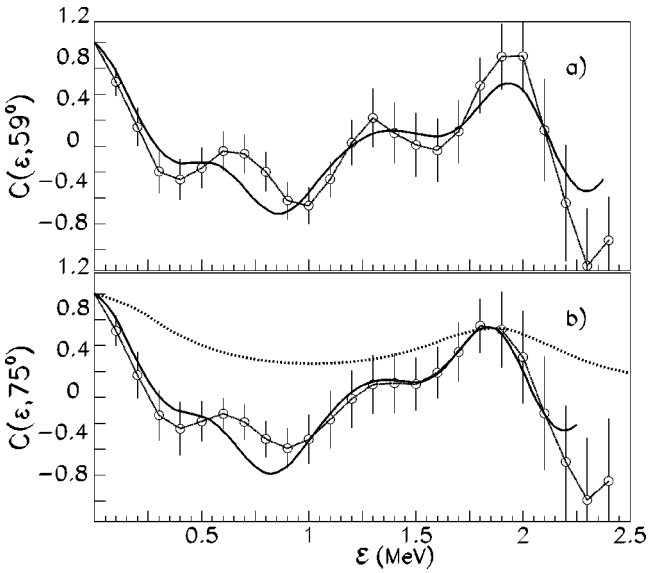

FIG. 11. (a) Experimental energy autocorrelation function (points) at $\theta = 59°$ compared with the theoretical one (thick line) as obtained by means of the POMLM with the parameters reported in Table I. (b) Like (a) but for $\theta = 75°$. The dotted line represents the theoretical prediction corresponding to the ''slow'' mechanism for the energy autocorrelation function computed in an energy interval $\Delta E \gg \hbar\omega$.

D. Energy autocorrelation functions and the model prediction

In Figs. 11(a) and 11(b) we show as an example a comparison between the experimental energy autocorrelation functions at $\theta = 59°$ and $\theta = 75°$ with the prediction of the model (continuous thick line) as obtained from the global fit procedure. The theoretical and experimental quantities agree well both for the shape and the position of the bump around 2 MeV. It has to be noted that, because of the FRD errors, the half width of the simulated energy autocorrelation is about 150 keV (comparable with the experimental value) while the limiting value, obtained for average energy intervals $\Delta E \gg \hbar\omega$, is about 450 keV. With more details the FRD errors connected to the model can be easily estimated by looking at the dotted curve of Fig. 11(b). This curve represents the energy autocorrelation related to the slow process (at 75° the slow process is more than two times the fast one) generated by the excitation function simulated on an energy interval of several tens of MeV, for which the errors arising from the FRD are negligible.

In the following sections we will discuss in detail the criterion used to fix the energy scale of the process together with a study of the sensitivity of the fluctuations properties to the model parameters characterizing the slow process.

E. Average angular velocity and total angular momentum

In Fig. 12(a) we display, by means of a continuous line, the results for the energy autocorrelation function at $\theta = 75°$ as obtained from the fit procedure [see Fig. 11(b)].

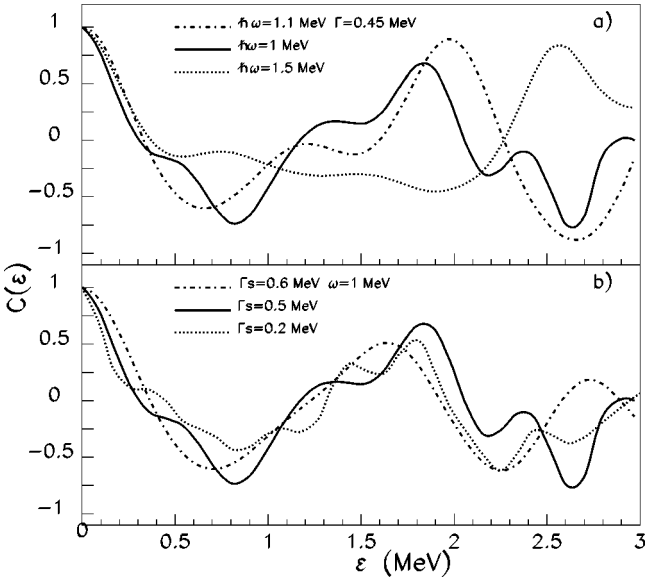

FIG. 12. (a) Energy autocorrelation function computed for different values of the $\hbar\omega$ parameter. The continuous line represents the calculation obtained through the global fit procedure. (b) Like (a) but for different values of the Γ_s parameter. The values of the parameter are reported in the figure.

In the same figure we show with dashed lines, calculations for which only the value of $\hbar\omega$ parameter has been changed to 1.1 and 1.5 MeV. All the calculations have been performed in a finite energy interval of about 3 MeV. The finite degree of angular momentum correlation produces an increase of correlation around an energy interval of about $2\hbar\omega$ (symmetric system). This effect is noticeable in the figure by looking at the average trend under the oscillations connected to the FRD of data (see next section). From the comparison with the experimental data we can estimate, inside a 10% of error, a value of about 1 MeV for the $\hbar\omega$ parameter.

Because we are not sensitive to the typical near-far side oscillations we cannot estimate the average angular momentum involved in the process. We also do not have direct information about the inertia parameter.

Therefore we can only make some comments about the estimated average angular velocity and the location of the *J* window.

For systems with a total mass of 56 amu, in the same region of excitation energy, the critical angular momentum momenta estimated through fusion cross section measurements in the sharp cutoff approximation is about $33\hbar$ [28]. This value is in good agreement with the evaluation performed for the system under study by using a Krappe Nix nucleus-nucleus potential [29]. If we suppose our process to be located around $33\hbar$ and considering an inertia parameter of a deformed system in the ''sticking'' configuration, we obtain a $\hbar\omega$ value of about 1.3 MeV. With this value it is not possible to reproduce the experimental energy autocorrelation functions.

On the other hand, by increasing the inertia parameter by 30% with respect to the ''sticking'' configuration (owing for example to the intrinsic deformation of the two nuclei) it is possible to recover the experimental value of $\hbar\omega=1$ MeV with $\bar{J}=33\hbar$.

This is close, within the experimental errors, to the value estimated for the similar system $^{28}Si+^{28}Si$ [19] in an equivalent energy interval. For that case, the estimation was rather direct: in fact, we used the period $\pi/\bar{J}$ of the oscillations appearing in the angular distribution connected to the near-far side interference effect in the inelastic processes. In the ''sticking'' limit of a dinuclear configuration, such a value of $\bar{J}$ corresponds to about $\hbar\omega\simeq 1$ MeV which, in turn, was in agreement with the time scale of the process.

Finally we observe that the energy domain explored in this work corresponds to the high energy limit of the so-called region II of the fusion excitation function [30–32]. In this energy domain, using also an approximation scheme above the simple sharp cutoff prescription, the possibility that total angular momenta lower than $33\hbar$ can also feed the binary inelastic channels through the so-called ''fast fission'' process, does not appear to be unreasonable. The higher values of *J*, which correspond to higher values of $\hbar\omega$, will instead probably feed the so-called ''fast'' process which is the main contribution detected at forward angles.

F. The other parameters for the slow process

Following the same criterion of the calculations presented in the previous section, in Fig. 12(b) we show, as an example, the results of calculations performed for the energy autocorrelation function at $\theta=75°$, in which the Γ_s parameter has been changed with respect to the value obtained from the fit procedure.

It is interesting to note that for $\Gamma_s\leqslant 0.6$ MeV oscillations of a period about 2Γ appear in the correlation function, superimposed on the average trend as a result of the FRD errors. This behavior, for such a small variation of the Γ parameter and small energy range, seems much more characteristic than the width at half maximum that one can extract from the initial part of the correlation function. The change of period between the case $\Gamma_s=0.2$ MeV and $\Gamma_s=0.5$ MeV is clearly visible.

A comparison with the trend shown by the experimental data [see Fig. 11(b)] suggests a value of about $\Gamma_s=0.5$ MeV with an uncertainty interval 0.2–0.6 MeV coming from the experimental errors.

Finally, in Fig. 13 we show the change of the simulated energy autocorrelation function for different values of the Δ_s parameter. In the small insert of Fig. 13 are also shown the corresponding calculations performed on an a very large energy interval.

The parameter Δ_s is connected with the average number of partial waves contributing to the process and determines the initial quantal dispersion of the wave packet. The continuous line which fits the experimental result is computed for $\Delta_s=2$, similar results inside the errors are obtained for Δ_s varying in the interval 2–4.

Noticeable differences are visible for $\Delta_s\leqslant 1$ and $\Delta_s\geqslant 5$.

For $\Delta_s\leqslant 1$ the energy autocorrelation function, as computed in the finite energy interval, exhibits only a periodicity of about 2Γ. In this case, in fact, practically only one partial

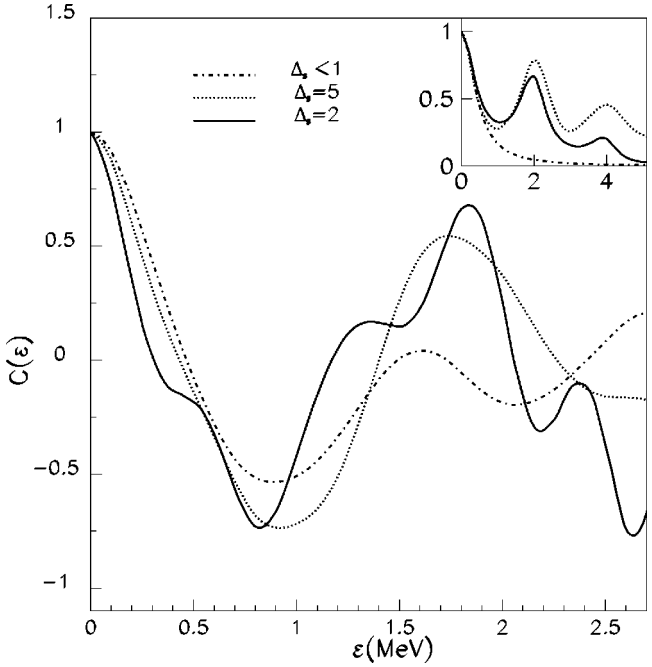

FIG. 13. Energy autocorrelation functions computed for different values of the Δ_s parameter. The corresponding values are reported in the figure. In the panel on the upper right side of the figure, the energy autocorrelation functions computed for the same set of parameters in an energy interval $\Delta E \gg \hbar\omega$ are also displayed.

wave contributes to the process and then there is not the possibility of observing the effect connected to the coherent rotation.

For $\Delta_s \geqslant 5$ the peak at about 2 MeV is clearly seen, while the oscillations connected to the mean level width are strongly damped.

The intermediate case, which corresponds well to the experimental findings, is the case in which the oscillations connected to the 2Γ periodicity are superimposed on the peak around 2 MeV. These oscillations represent a noise and, on the large energy scale, they will generate a lower correlation around 2 MeV with respect to the case corresponding to a higher value of Δ. This effect can be understood in terms of angular localization of the intermediate complex at the moment of contact which, for large values of the Δ parameter (see Sec. V C), permits a sharper time separation (a more narrow angular localization of the intermediate system) of the contribution coming from the decay after a rotation of 2π [16]. This, in turn, will generate a higher peak around 2 MeV and also a higher visibility (ratio between maximum and minimum) as can be seen in the panel.

In the same inset of Fig. 13 it can be also observed that the second peaks, connected to the second turn of the intermediate complex, are wider and weaker than the first one because of the results of the spontaneous spreading of the wave packet (see Sec. IV) which try to destroy the coherent rotation.

The dependence of the fluctuation behavior in this case is weak with respect to the Φ_s parameter. This is justified by the relatively low degree of coherence ($\gamma_s \simeq 0.5$) which reduces the sensitivity of the correlation functions to the initial orientation of the intermediate complex. On the other hand because Φ_s is connected to the average potential phase shift, we can reasonably assume $\Phi_s \simeq \Phi_f$.

Before concluding this section, we want to stress that the study of the correlation functions through simulations on finite energy interval allows us to understand the way in which the information is modified by the FRD errors with respect to the ideal and extreme case in which an infinite energy interval is available. This extreme case is exactly that in which closed analytical expression can be eventually obtained.

This study in particular shows that the way in which the information is distorted still depends on the parameters of the model and highlights, as in our case, periodicity (that connected to the mean level width) which is not present in the correlation function evaluated in the above mentioned ideal case (see inset of Fig. 13). *Therefore any reliable comparison between the experimental quantities and models should not undervalue this aspect.*

G. Amplitude of the fluctuation and molecular level density

For a symmetric system and for a finite value of the γ parameter, the behavior of the square root of the normalized variance V computed in a very large energy interval in presence of an uncorrelated fast process, can be approximated by the following relation:

$$V = 1.5^{*}(\Delta)^{\frac{-1}{\gamma+1}} \frac{\sigma_s(\theta)}{\sigma_s(\theta)+\sigma_f(\theta)} \sqrt{\frac{D}{\Gamma}}. \tag{9}$$

This expression takes into account the change of V with the number of partial waves contributing to the cross section and with their degree of coherence (Δ's and γ's dependence), and finally, the dependence on the level density of states with a fixed total spin (see the Appendix).

For a finite energy interval of about 3 MeV and for the parameters values deduced by the previous analysis, the results obtained by performing several simulations confirm that, because of the FRD errors, V is reduced of a factor about $\frac{1}{2}$.

Substituting the parameters obtained from the previous analysis into the relation (9), the experimental values in the angular range 47°–79° are reproduced within the experimental errors by setting a value of Γ_s/D_s of about 13. In Fig. 5 we show the comparison between the experimental data (full dots) and the calculations (open dots). Within the errors the agreement is good for $\theta \geqslant 47°$.

Because of the errors on the parameters estimated in the previous sections, considering also the uncertainty arising from the experimental data and from the energy behavior of the underlying fast contribution, we can estimate an interval of uncertainty on the Γ_s/D_s value from 10 to 40.

As mentioned in Sec. V B, the excitation functions show a visible trend variation with energy only in the forward part of the explored angular range. This is a signal of the existence of a fast process dominating the forward region (this consideration is independent from any model). In the framework of the approach used, this evidence can be justified only by supposing also a finite value of the ratio Γ_f/D_f

which we have set to about 5 (with $\Gamma_f = \gamma_f \hbar\omega$). This value allows us to reproduce, within the errors, the variance at 43°, but, because of the relative small energy interval of measurements, this value can have a high degree of uncertainty.

At smaller angles where the fast process is predominant the agreement between the calculation and the observed variances is poor. Nevertheless we have to observe that the experimental results concerning the fluctuations measurement in the forward part are critical. Apart from the ^{12}C contamination problem a very small beam displacement verified during the change of the beam energy (the displacement could be at the most 1 mm according to the collimation system we have used) could generate in this angular region a $\delta\theta$ of the order of a fraction of a degree (see Sec. I) which, in turn, can produce variation in the cross sections of the same order of magnitude of the fluctuations we are discussing. This is due to the fact that the change of the angular distribution is very fast in the forward region. Obviously this kind of effect has a negligible consequence on the determination of the experimental average angular distribution whose measurement in an as wide as possible angular range is of fundamental importance to determine the relative percentage of the fast contribution with respect to the slow one.

H. Angular correlation function

Finally we comment on the results shown in Figs. 8(a) and 8(b). The angular region for $\theta < 47°$ is not reproduced by the model calculations. As previously observed this angular region can be critical for the fluctuations analysis for our experimental setup because of the fast changes of the average angular distribution. Concerning the remaining explored angular range the agreement between the experimental points and the POMLM is, taking into account the errors, good.

To understand better the results obtained by the model we can refer to the following general expression for the angular correlation function connected to a cross section composed of two incoherent contributions:

$$C(\theta,\theta') = \frac{A(\theta,\theta')}{B(\theta)B(\theta')},$$

$$\begin{aligned} A(\theta,\theta') = {} & C_f(\theta,\theta')V_f(\theta)V_f(\theta') \\ & + C_s(\theta,\theta')V_s(\theta)V_s(\theta')K(\theta)K(\theta') \\ & + C_{f,s}(\theta,\theta')(V_f(\theta)V_s(\theta')K(\theta') \\ & + V_f(\theta')V_s(\theta)K(\theta)), \end{aligned}$$

$$\begin{aligned} B(\theta) = {} & (V_f^2(\theta) + V_s^2(\theta)K(\theta)^2 \\ & + 2C_{f,s}(\theta)V_s(\theta)V_f(\theta)K(\theta))^{1/2}, \end{aligned} \tag{10}$$

where V_f, V_s indicates the square root of the variance for the fast and slow process, respectively, K indicates the ratio between the slow and the fast contribution, C_f, C_s indicate the angular correlation of the two contributions, and $C_{f,s}$ indicates the angular correlation between the two processes.

For the set of parameter given in Table I and according to the observation made at the end of Sec. III the POMLM predictions are the following: $V_f(\theta)$ changes from 1.2×10^{-2} to 4.5×10^{-2} for θ varying in the explored angular range; $V_s(\theta) \simeq 7 \times 10^{-2}$; $C_s(\theta,\theta') \simeq 1 (\gamma_s < 1)$.

The values of $C_f(\theta,\theta')$ and $C_{f,s}(\theta,\theta')$ both depend on the choice of the starting seeds which generate the level sequence and the partial amplitude in Eq. (5). To fit the behavior of the experimental $C(55°,\theta)$ the seeds have been selected to obtain a $C_{f,s}(55°,55°)$ value of about -0.38. We would like to stress that the strong dependence on the chosen level sequence of the correlation between the fast and slow process means that in the incident energy range δE under study, the FRD errors on the $C_{f,s}(55°,55°)$ parameter connected with the fast process ($\Delta E \simeq \Gamma_f$), are dominant.

Nevertheless, it is important to observe also that at backward angles, independently from the seeds, and for the energy interval under study, the change of the angular correlation depends practically on the $K(\theta)$ coefficients which, on the other hand, are determined by the angular distribution fit procedure. This happens because at angles where the slow process is dominant ($\theta \geqslant 55°$) the change of the angular correlation is very small [$C_s(\theta,\theta') \simeq 1$]. This behavior is particularly evident in Fig. 8(b) where, the reference angle being equal to 67°, the theoretical $C(\theta,\theta')$ for $\theta' > 67°$ is equal practically to one while the experimental data shows a slightly decreasing trend.

This result mainly depends on the fact that in the POMLM the off-diagonal elements with respect to the total angular momentum quantum number are small and strongly correlated for the slow process. This behavior can in turn depend on the following approximations for the level structure and partial amplitudes: (a) $E_\mu^J = (\hbar^2/2I)J(J+1) + E_\mu^0$; (b) the partial amplitudes $\gamma_{\alpha,\mu}$ are presumed to be independent on J.

These conditions imply that all the levels follow the same rotational band and no coupling between the collective rotation of the intermediate system and the other intrinsic degree of freedom exists. The introduction of the coupling effects, able to produce a loss of angular correlation in processes of low degree of angular momentum coherence, modeled with a random dependence of the partial amplitude $\gamma_{\alpha,\mu}^J$ from J, will be the concern of the future developments of the approach used.

VI. LEVEL DENSITY AND THE POMLM

As already mentioned in Sec. IV the main hypothesis underlying the theoretical approach used is that many partially overlapped resonances coherently contribute to the phenomenon under study. In this section we want to discuss briefly the possible existence of such kinds of states and their nature.

The fit procedure of the experimental data allows us to extract an average angular velocity $\hbar\omega \simeq 1$ MeV. The average value of the total angular momentum is not well defined and, according to the observation of Sec. V E, this value may be located inside a probable window 26–$34\hbar$. This window corresponds to an average collective rotational energy

$E_{\mathrm{rot}}(\bar{J})=(\hbar\omega/2)\bar{J}$ varying within the interval 13–17 MeV.

We can also express, according to the collective rotation picture, the ''zero temperature'' rotational band through the following expression:

$$E_B(J)=E_{\mathrm{rot}}(J)+Bf-Q_0, \tag{11}$$

where Bf is the barrier for symmetric fission of the system and Q_0 is the Q value for fusion. $Bf-Q_0$ can represent therefore in a reasonable way the energy necessary to produce a strongly deformed system at the scission point configuration.

Taking into account the interval of possible average rotational energy values, as previously estimated, the fraction of intrinsic excitation energy ($E_{\mathrm{c.m.}}\simeq 60$ MeV) that can be absorbed by the system, above the ''zero temperature'' rotational energy, can vary in the interval 12–17 MeV. At this excitation energy the level density, as evaluated by means of the Fermi gas model, is much higher than the values estimated to reproduce the amplitude of the cross section fluctuations (see Sec. V G).

For example for $E^*=15$ MeV and $\bar{J}=33\hbar$, the Fermi gas model predicts a level density of the order of 5×10^5 MeV^{-1}. Moreover, the associated decay width as estimated from the Weisskopf formula is of the order of 10 keV for particle emission. On the other hand, the study of the experimental energy autocorrelation functions allow us to estimate an average level width of a few hundred keV (200–500 keV; see Sec. IV F) indicating a prominent binary decay mode, through states characterized by a finite degree of angular momentum coherence ($\gamma\simeq 0.5$).

All these considerations strongly suggest that the states responsible for the fluctuations should be considered as special ones with a density very different from the previously mentioned value.

The POMLM predicts through the analysis performed in the present work a density of states for the slow process ranging approximately in the interval 20–90 MeV^{-1} (for $\Gamma_s=0.5$ MeV). From a macroscopic point of view these special states could have the same nature as the so-called dinuclear molecular states (see for example [33–37]) which, at a relatively high intrinsic excitation energy (13–17 MeV), can become partially overlapped. From a microscopic point of view they could be addressed to simple coherent particle-hole excitations which act as ''door way states'' for the process under study.

In this respect we may cite the studies connected to the multistep preequilibrium reaction theory of particles-nucleus interaction in which the estimation of the partial level density and their damping width evaluated in the framework of the single particle model play a fundamental role. As an example, in Ref. [38] the partial level density in ^{40}Ca of 2p-2h and 3p-3h excitations of low spin was estimated at $E^*=10$–20 MeV to vary in the range 1–50 MeV^{-1}. In Ref. [39] Hermann *et al.* evaluate the damping width for ^{94}Nb at $E^*=20$ MeV connected to such a simple configurations as to be of the order of 1.5 MeV and 500 keV for the 2p-2h and 3p-3h excitations, respectively.

Unfortunately the above consideration can be up to now only of qualitative character because of the lack of a microscopic quantum-theory of the heavy ion interaction.

VII. CONCLUDING REMARKS

The fluctuations in the excitation functions of dissipative binary collision induced on the ^{27}Al+^{27}Al at $E_{\mathrm{lab}}=114$–124 MeV with step 200 keV have been analyzed in the framework of the POMLM. In the approach used, no correlations between the amplitudes connecting the initial state to the very high number of final microchannels populated in the dissipative process have been considered, but the correlation necessary to explain the fluctuations is produced through the excitation of quasimolecular levels of low density. In this work all the quantities characterizing the phenomenon, average angular distribution normalized variance, energy autocorrelation functions and angular correlation functions have been interpreted by means of a most probable set of model parameters as the result of a coherent rotation of the highly deformed intermediate system formed in a narrow total angular momentum window. The experimental data correspond, in many respects, to the combined effect of two uncorrelated mechanisms labeled by two different characteristic times or in an equivalent way by two different energy coherence lengths $\Gamma_f\geqslant 2.7$ MeV and $\Gamma_s\simeq 0.5$ MeV.

The comparison between the experimental angular correlation and the model predictions provides some evidence that the coupling between the rotational degree of freedom and the other ones has to be considered. This subject will be the concern of the future development of the POMLM. The above mentioned evidence suggests that an improvement of the model can be obtained using a stochastic modelling of the S matrix decomposition with respect to the total spin.

The approach used allows us to obtain information on some quantities connected to the macroscopic or collective characterization of the intermediate system like the average angular velocity (in some cases also the average value of the total angular momentum involved in the process [19]) and some others connected to the microscopic structures like the mean decay width of the decaying dinuclear system, the average level density of the excited states through which the phenomenon evolves.

In this respect, partial level density estimations and decay width evaluations in static single particle model calculations [38,39], performed for high spin and very deformed systems, may be enlightening in the global understanding of the process and in particular in the microscopic description of the IDS formed during the first moments of a dissipative collision.

Finally we would like to stress that the fit procedure has clearly shown the very important role played by the simulations performed according to the approach used to take into account the effect arising from the FRD errors, and furthermore how the associated uncertainty on the fit parameters can be partially recovered also by studying all the quantities characterizing the fluctuations in the excitation functions.

ACKNOWLEDGMENTS

Thanks are due to C. Marchetta for the high quality targets and to S. Marletta for the high stability source. We are also grateful to Dr. J.S. Winfield for the careful reading of the manuscript and comment.

APPENDIX

Let us write the total cross section as

$$\sigma(E,\theta)=\sum_{\beta}\sigma_{\alpha,\beta}(E,\theta)$$

$$\propto\sum_{J,J'}(2J+1)(2J'+1)(W(J')W(J'))^{1/2}$$

$$\times\sum_{\mu}\sum_{\mu'\beta}\frac{b^{\beta}_{\alpha,\mu}b^{*,\beta}_{\alpha,\mu'}e^{(\phi(J)-\phi(J'))}}{D(E,\mu,J)D(E,\mu',J')^{*}}P_{J}(\theta)P_{J'}(\theta), \tag{A1}$$

where

$$D(E,\mu,J)=E-E_{\mu}-E_{\mathrm{rot}}(J)-i\frac{\Gamma}{2}.$$

The numbers $b^{\beta}_{\alpha,\mu}$ are random variables characterized by the following properties: (i) $\langle b^{\beta}_{\alpha,\mu}\rangle=0$ and $\overline{b^{\beta}_{\alpha,\mu}}=0$; (ii) $b^{\beta}_{\alpha,\mu}b^{\beta'}_{\alpha,\mu'}=\delta_{\mu,\mu'}\delta_{\beta,\beta'}\overline{|b^{\beta}_{\alpha,\mu}|^{2}}$.

The brackets indicate the average over the level μ while the bars indicate the average over the final channels. The first conditions state that the amplitudes $b^{\beta}_{\alpha,\mu}$ are random with respect to the μ and β indexes; the second one means that even if the correlation between two generic final channels can be different from zero, the average over all the very large number of distinct couples is zero. Without losing generality we can consider the numbers $b^{\beta}_{\alpha,\mu}$ to be real.

We concentrate on the μ' and β sum:

$$\sum_{\mu',\beta}\frac{b^{\beta}_{\alpha,\mu}b^{\beta}_{\alpha,\mu'}}{D(E,\mu,J)D(E,\mu',J')^{*}}$$

$$=\sum_{\beta}\frac{|b^{\beta}_{\alpha,\mu}|^{2}}{D(E,\mu,J)D(E,\mu,J')^{*}}$$

$$+\sum_{\mu'\neq\mu,\beta}\frac{b^{\beta}_{\alpha,\mu}b^{*,\beta}_{\alpha,\mu'}}{D(E,\mu,J)D(E,\mu',J')^{*}}$$

$$=A_{\mu}+B_{\mu}. \tag{A2}$$

First of all we perform the summation over the final channels. The average value $\overline{A_{\mu}}$ of A_{μ} can be estimated as

$$\overline{A_{\mu}}=\frac{\overline{|b^{\beta}_{\alpha,\mu}|^{2}}N}{D(E,\mu,J)D(E,\mu,J')^{*}}, \tag{A3}$$

where N is number of final channels and $\overline{|b^{\beta}_{\alpha,\mu}|^{2}}=\Sigma_{\beta}|b^{\beta}_{\alpha,\mu}|^{2}/N$.

Its standard deviation is

$$\delta A_{\mu}=\frac{\overline{|b^{\beta}_{\alpha,\mu}|^{2}}\sqrt{N}\chi}{D(E,\mu,J)D(E,\mu,J')^{*}}, \tag{A4}$$

where χ is the standard deviation on the numbers $|b^{\beta}_{\alpha,\mu}|^{2}$ with respect to the β index.

Now we evaluate the mean value and its fluctuation for the term B_{μ}. This term generates the off-diagonal element of the expression (A1).

To this aim we consider the random variable

$$\sum_{\beta}b^{\beta}_{\alpha,\mu}b^{\beta}_{\alpha,\mu'}=\sum_{\beta}Y^{\beta}_{\mu,\mu'}=Y^{S}_{\mu,\mu'}$$

from the conditions (ii); it results that its most probable value is 0 with a standard deviation $\sqrt{N}\chi_{Y}$ where χ_{Y} is the standard deviation of the product $b^{\beta}_{\alpha,\mu}b^{\beta}_{\alpha,\mu'}$ with respect to the index β.

For a fixed realization of the sum S we have now to evaluate the mean value and fluctuation for the sum over μ'. We consider the stochastic variable:

$$L^{S}_{\mu,\mu'}=\frac{Y^{S}_{\mu,\mu'}}{D(E,\mu,J)D(E,\mu',J')^{*}}. \tag{A5}$$

By assuming an uncorrelated numerator and denominator, it results that the average value of all the possible construction of the sum with respect to μ' is zero, i.e.,

$$\tilde{Z}_{\mu}=\sum_{\mu'}\tilde{X}'^{,S}_{\mu,\mu'}=0. \tag{A6}$$

Because the number of dominant terms in the expression (5) is of the order of Γ/D we can estimate the standard deviation on the Z_{μ} variable to be of the order

$$\delta Z_{\mu}\propto\sqrt{\frac{\Gamma}{D}}\sqrt{N}\chi'. \tag{A7}$$

If Γ/D is finite, in the limit $N\rightarrow+\infty$, for each μ level, for each energy and pair of total spin J,J', the sum of the off-diagonal elements of expression (A1) is negligible with respect to the mean value of the μ diagonal element at the order of $1/\sqrt{(N)}$.

This means that we can write the total cross section as

$$\sigma(E,\theta)=\sum_{\beta}\sigma_{\alpha,\beta}(E,\theta)$$

$$\propto\sum_{J,J'}(2J+1)(2J'+1)(W(J')W(J'))^{1/2}\times\sum_{\mu}\frac{\overline{|b^{\beta}_{\alpha,\mu}|^2}e^{(\phi(J)-\phi(J'))}}{D(E,\mu,J)D(E,\mu,J')^*}P_J(\theta)P_{J'}(\theta), \tag{A8}$$

which coincides with Eq. (5) (see text).

As function of the energy this expression shows a fluctuating behavior for finite values of the ratio Γ/D at the order of $\sqrt{D/\Gamma}$ around its mean value.

For $\Gamma/D\rightarrow+\infty$ (i.e., Γ/D at least as large as the same order of N), the off-diagonal elements can not be in principle neglected term by term. Then we perform the sum over the μ index. For each energy value and couple of total spin we write

$$\sum_{\mu}\frac{\overline{|b^{\beta}_{\alpha,\mu}|^2}N}{D(E,\mu,J)D(E,\mu,J')^*}=\frac{\Gamma}{D}N\left\langle\frac{\overline{|b^{\beta}_{\alpha,\mu}|^2}}{D(E,\mu,J)D(E,\mu,J')^*}\right\rangle. \tag{A9}$$

The factor Γ/D in Eq. (A9) represents approximately the number of terms contributing to the sum.

Because of the already mentioned statistical hypothesis on the partial amplitude $b^{\beta}_{\alpha,\mu}$, the contribution associated to the sum of the off-diagonal terms will have a zero average with a standard deviation of the order of $\sqrt{\Gamma/D}\sqrt{\Gamma/D}\sqrt{(N)}\chi'$.

We therefore once more obtain that if the number of final channels is very large, the sum of the off-diagonal terms can be neglected with respect to the sum of the diagonal ones for each energy at the order $1/\sqrt{(N)}$ and then Eq. (A8) is valid.

We want to conclude by observing that the total cross section has been expressed in Eq. (A1) through the sum of the square modulus of the amplitudes connecting the different channels, i.e., the interference effects between them have been neglected. This interference effect should have a zero average value [according to the assumptions (i) and (ii)] but, by using the same argument as above, the different realizations of the sum can produce fluctuations of the order of N' where N' is number of final channels which are in principle indistinguishable.

We can estimate this number to be of the order $N'=N(\Gamma_{\beta}/\Delta Q)$ where Γ_{β} is the typical width of the primary metastable fragments produced, while ΔQ is the Q-value window in which the total cross section is integrated. In our case we can have Γ_{β} of the order of 10 keV and $\Delta Q=20$ MeV, so we may estimate that the random nature of the interference between the different channels will give a contribution of 3 orders of magnitude smaller than the incoherent sum of the amplitudes. Moreover, we have to consider the averaging effect connected with experimental apparatus always being characterized by response functions that have finite widths. This averaging effect will produce a reduction of the statistical interference contribution at the order $\sqrt{N'}$.

These two arguments allow us to express the total cross section through Eq. (A1).

[1] A. De Rosa, G. Inglima, V. Russo, M. Sandoli, G. Fortuna, G. Montagnoli, C. Signorini, A.M. Stefanini, G. Cardella, G. Pappalardo, and F. Rizzo, Phys. Lett. **160B**, 239 (1985).

[2] M.C. Mermaz, T. Suomijarvi, R. Lucas, B. Berthier, J. Matuszec, J.P. Coffin, G. Guillaume, B. Hensch, F. Jundt, and F. Rami, Nucl. Phys. **A456**, 186 (1986).

[3] T. Suomijarvi, B. Berthier, R. Lucas, M.C. Mermaz, P. Coffin, G. Guillaume, B. Hensch, F. Jundt, and F. Rami, Phys. Rev. C **36**, 181 (1987).

[4] G. Pappalardo, Nucl. Phys. **A488**, 395c (1988).

[5] T. Ericson, Ann. Phys. (N.Y.) **23**, 390 (1963).

[6] D.M. Brink and K.Z. Dietrich, Z. Phys. A **326**, 7 (1987).

[7] S.Yu. Kun, M. Papa, and D.K. Sunko, Phys. Lett. B **249**, 1 (1990).

[8] S.Yu. Kun, Phys. Lett. B **257**, 247 (1991).

[9] S.Yu. Kun and W. Nörenberg, Z. Phys. A **343**, 215 (1992).

[10] S.Yu. Kun, W. Nörenberg, and M. Papa, Phys. Lett. B **298**, 273 (1993).

[11] S.Yu. Kun, M. Papa, and A.B. Robson, Z. Phys. A **347**, 123 (1993).

[12] G. Cardella, M. Papa, G. Pappalardo, F. Rizzo, A. De Rosa, G. Inglima, and M. Sandoli, Z. Phys. A **332**, 195 (1989).

[13] A. De Rosa, E. Fioretto, G. Inglima, M. Romoli, M. Sandoli, G. Cardella, M. Papa, F. Rizzo, D.R. Napoli, A.M. Stefanini, and C. Signorini, Phys. Rev. C **44**, 747 (1991).

[14] G. Cardella, M. Papa, G. Pappalardo, F. Rizzo, Wang Qi, A. De Rosa, E. Fioretto, G. Inglima, M. Romoli, M. Sandoli, R. Setola, L. Corradi, G. Montagnoli, D.R. Napoli, and A.M. Stefanini, Z. Phys. A **336**, 387 (1990).

[15] Wang Qi, Lu Jun, Xu Hushan, Li Songlin, Zhu Yongtai, Fan Enjie, Yin Xu, Zhang Yuhu, Guo Zhongyan, Zhu Yongtai, Li Zhichang, Zhao Kui, Lu Xiuqin, and Hu Xiaoqing, Phys. Lett. B **388**, 462 (1996).

[16] G. Pappalardo and M. Papa, in *Proceedings of the Workshop on Multistep Direct Reaction, NAC FAURE S.A., 1991*, edited by R.H. Lemmer (World Scientific, Singapore, 1992), p. 89.

[17] M. Papa, Ph.D. thesis, VI Cycle, Catania University, 1994.

[18] F. Rizzo, G. Cardella, A. De Rosa, A. Di Pietro, A. D'Onofrio, E. Fioretto, G. Inglima, A. Musumarra, M. Papa, G. Pappalardo, M. Romano, F. Terrasi, M. Sandoli, and G.S. Wang, Z. Phys. A **349**, 169 (1994), and references therein.

[19] M. Papa, G. Cardella, A. Di Pietro, A. Musumarra, Li Songlin, A. De Rosa, G. Inglima, M. La Commara, D. Pierroutsakou, and M. Romoli, Z. Phys. A **353**, 205 (1995).

[20] I. Bercenau *et al.* Phys. Rev. C **57**, 2359 (1998).

[21] F. Puhlhofer, Nucl. Phys. **A280**, 267 (1977).

[22] S.Yu. Kun, Z. Phys. A **357**, 271 (1997).
[23] G. Pappalardo, Phys. Lett. **13**, 320 (1964).
[24] J.J.M. Verbaarshcot, H.A. Weindenmuller, and M.R. Zirimbauer, Phys. Rep. **129**, 367 (1985).
[25] C.H. Lewenkops and H.A. Weindenmuller, Ann. Phys. (N.Y.) **212**, 53 (1991).
[26] C.E. Porter, *Statistical Theories of Spectra Fluctuations* (Academic, New York, 1965).
[27] V.M. Strutynsky and S.M. Vydrug-Vlasenko, Z. Phys. A **294**, 281 (1980).
[28] S.M. Lee, T. Matsuse, and A. Arima, Phys. Rev. Lett. **45**, 165 (1980).
[29] H.J. Krappe, J.R. Nix, and A.J. Sierk, Phys. Rev. C **20**, 992 (1979).
[30] D.G. Kovar *et al.*, Phys. Rev. C **20**, 1305 (1979).
[31] D. Glass and U. Mosel, Nucl. Phys. **A237**, 429 (1975).
[32] J.A. Cameron, D.G. Popescu, and J.C. Waddington, Phys. Rev. C **44**, 2358 (1991).
[33] N. Cindro, Ann. Phys. (N.Y.) **13**, 289 (1988).
[34] U. Abbondanno, Phys. Rev. C **43**, 1484 (1991).
[35] R.R. Betts, B.B. Back, and B.G. Glagola, Phys. Rev. Lett. **47**, 23 (1981).
[36] R.R. Betts, S.B. DiCenzo, and J.F. Peterson, Phys. Lett. **100B**, 117 (1981).
[37] E. Uegaky and Y. Abe, Phys. Lett. B **340**, 143 (1994).
[38] K. Sato, Y. Takahashi, and S. Yoshida, Z. Phys. A **339**, 129 (1991).
[39] M. Herman, G. Reffo, and H.A. Weidenmuller, Nucl. Phys. **A356**, 124 (1992).